Preparation and Characterization of Poly(vinylidene fluoride) Hollow Fiber Membranes for Vacuum Membrane Distillation

Bing Wu,[1] K. Li,[2] W. K. Teo[3]

[1]*Department of Chemical and Biomolecular Engineering, National University of Singapore, Singapore 119260*
[2]*Department of Chemical Engineering, Imperial College London, University of London, SW7 2AZ, United Kingdom*
[3]*Division of Chemical and Biomolecular Engineering, Nanyang Technological University, Singapore 637722*

Received 13 July 2006; accepted 11 September 2006
DOI 10.1002/app.26624
Published online 16 July 2007 in Wiley InterScience (www.interscience.wiley.com).

ABSTRACT: Various asymmetric microporous poly(vinylidene fluoride) (PVDF) hollow fiber membranes with different pore sizes and effective porosities were prepared by the phase inversion method using dimethylacetamide (DMAc) as solvent and LiCl and water as additives. The membranes were characterized using scanning electron microscopy (SEM) and field emission scanning electron microscopy (FESEM) for its microstructure and surface pore size. A gas permeation method was also applied for determining and comparing the effective surface porosity and mean pore size of the different membranes. Moreover, the contact angle with water, critical entry pressure (CEP) of water and collapsing pressure of the PVDF hollow fibers were also determined. Five membrane modules were prepared using the spun hollow fibers and applied in removing 1,1,1-trichloroethane (TCA) from its aqueous solution by vacuum membrane distillation (VMD) process. The effects of dope composition and spinning conditions on hollow fiber morphology and TCA separation by VMD process are examined. Post-treating of the spun fibers by solvent exchange using ethanol produced membranes exhibiting higher porosity and higher permeability. A highly porous hollow fiber membrane with a smaller mean pore size can achieve both high TCA permeation flux and high separation factor. © 2007 Wiley Periodicals, Inc. J Appl Polym Sci 106: 1482–1495, 2007

Key words: membranes; morphology; fluoropolymers; additives; separation techniques

INTRODUCTION

Membrane distillation (MD) is a separation process in which a heated aqueous solution is brought into contact with one side of a microporous hydrophobic membrane, and the hydrophobic nature of the membrane prevents the penetration of the aqueous solution into the pores of the membrane, resulting in a vapor-liquid interface at each pore entrance. The vapor pressure differences of permeating species across the membrane are the driving force in MD. MD process has been applied in desalination, removal of volatile organic compounds (VOCs) from waste water and in concentration of ionic, colloid, fruit juice, or other relatively nonvolatile aqueous solutions. The basic principles of MD was firstly described by Bodell in a U.S. patent in early 1963,[1] and the first MD publication was made by Findley in 1967.[2] Although the concept of MD has been known for about 40 years, the process is still in its development stage. An important and extensive historical review of MD was reported by Lawson and Lloyd in 1997[3] and more recently this membrane separation process was also reviewed by Burgoyne and Vahdati in 2000,[4] and Curcio and Drioli in 2005.[5]

Since the hydrophobic character of the membrane is an essential requirement of a MD process, membranes have to be prepared from polymers with a low value of surface energy. Poly(propylene) (PP), polytetrafluoroethylene (PTFE) and poly(vinylidene fluoride) are the three polymers commonly employed in the preparation of membranes for MD applications. Generally, the pore sizes of MD membranes range from 0.01 to 1 μm. Details of polymeric membranes used in membrane distillation are given by Burgoyne and Vahdati.[4] Commercial microporous flat-sheet or capillary hydrophobic membranes made from PP, PTFE, and PVDF, which are widely prepared for microfiltration purposes, have been commonly applied in MD experiments as summarized by Khayet, et al.[6] However, only a limited studies has been made on the preparation of membranes specially for MD applications.[6–13]

Wu et al.[7] surface-modified hydrophilic flat-sheet membranes of cellulose acetate and cellulose nitrate by radiation grafting polymerization and plasma polymerization into hydrophobic membranes, which were shown to possess good hydrophobicity required for MD process. Similarly, Kong et al.[8] prepared hydrophobic microporous composite membrane composed

Correspondence to: W. K. Teo (wkteo@ntu.edu.sg).

Journal of Applied Polymer Science, Vol. 106, 1482–1495 (2007)

of a hydrophilic layer sandwiched between two hydrophobic layers via plasma polymerization of octafluorocyclobutane on the two surfaces of cellulose nitrate microfiltration membrane. Fujii et al.[9] prepared PVDF hollow fiber membranes with mean pore size of several nanometers from binary solutions of PVDF/dimethyl sulfoxide by dry-jet wet-spinning method and applied them in direct contact membrane distillation (DCMD) experiments to study the permeability and selectivity of ethanol and water. They also studied the effect of coating and heat treatment of the PVDF membranes on the selectivity in DCMD experiments.[10] Ortiz de zárate[11] reported the performance of asymmetric flat-sheet membranes prepared from binary solutions of PVDF/dimethyl acetamide (DMAc) and PVDF/dimethylformamide (DMF) via phase inversion process in DCMD experiments. Tomaszewska[12] also prepared flat-sheet microporous PVDF membranes via phase inversion method from binary solutions of PVDF/DMF or ternary solutions of PVDF/DMAc/LiCl and tested the membrane performance in MD to treat aqueous NaCl solution. However, in their study, the PVDF membrane prepared with LiCl as an additive had a poor mechanical strength due to a very low PVDF concentration of 8 wt % and addition of LiCl. Khayet and Matsuura[13] used water as a pore-forming additive to prepare flat-sheet PVDF membrane from polymer dopes of PVDF/DMAc/H_2O for MD process. They recently reported the application of porous composite hydrophobic/hydrophilic membranes in DCMD. The composite membranes were prepared in a single casting step by the phase inversion method using polyetherimide (PEI) dope blended with surface-modifying macromolecules (SMM).[6]

Despite the various studies reported above, detailed studies on the preparation of porous hydrophobic membranes and membrane modules especially designed for MD applications are still lacking. In this study, several microporous asymmetric PVDF hollow fiber membranes were prepared via phase inversion method from polymer dopes containing DMAc as a solvent and a mixture of LiCl and H_2O as additives. Membranes with different pore sizes and porosities were prepared by varying the dope composition and spinning conditions. Membrane modules fabricated from five different types of membranes were applied in vacuum membrane distillation (VMD) process for the removal of 1,1,1-trichloroethane (TCA) from water. The performance of the membranes in the VMD process was evaluated with respect of the different membrane preparation conditions and parameters.

EXPERIMENTAL

Materials

Kynar K760 poly(vinylidene fluoride) polymer (PVDF, MW = 444,000) in pellet form was purchased from Elf Autochem (USA) and were pre-dried at 80°C for at least 8 h before use. Dimethyl acetamide (DMAc, ≥99%, synthesis grade) was used as a solvent. A mixture of LiCl (≥99%, ACS reagent grade) and deionized water was used as an additive. 1,1,1-trichloroethane (TCA, ≥99.5%, analysis grade) was used as the target VOC to be removed from its aqueous solutions in VMD process. All chemicals were purchased from Merck and used as received. In the spinning of hollow fibers, tap water was used as both internal and external coagulants.

Membrane preparation and characterization

Preparation of polymer dopes

A polymer dope solution was prepared by firstly mixing a required amount of solvent DMAC and solid LiCl in a 1-L wide neck flask immersed in a water bath maintained initially at 25°C. The mixture was stirred until LiCl was completely dissolved. A predetermined amount of PVDF polymer pellets was then introduced into the solvent and stirred at a low speed of 150 rpm at 25°C for half an hour to thoroughly wet the polymer pellets and prevent the formation of polymer lump. After that, the water-bath temperature was slowly raised from 25 to 60°C and the stirring speed was increased to 300 rpm. The agitation was continued until the PVDF pellets were completely dissolved into the solvent. The nonsolvent additive, water, was finally added into the polymer dope and stirred until a homogeneous solution with no visual turbidity was obtained. The polymer dope solution was cooled down to the room temperature (25°C ± 1°C) and a small portion of it was taken for viscosity measurements by a falling ball viscometer (HAAKE). Three different dope compositions (D15, D18, and D20) were prepared and are shown in Table I.

Spinning of hollow fibers

PVDF hollow fiber membranes were prepared by a wet-phase inversion method. The spinning apparatus and detailed spinning procedure can be found elsewhere.[14] A concise description is as follows: The fibers were spun through a spinneret with an orifice

TABLE I
PVDF Dope Compositions and Properties

Membrane dope	D15	D18	D20
PVDF (wt %)	15.00	18.00	20.00
DMAc (wt %)	77.83	75.90	75.00
H_2O (wt %)	1.95	1.67	1.37
LiCl (wt %)	5.22	4.43	3.63
Additive (g/100g solution)	7.72	6.50	5.26
Viscosity (mPa.s at 25°C)	2540	5260	6400

TABLE II
Spinning Conditions and Properties of the Resulting PVDF Hollow Fibers

Hollow fibre	F1	F2	F3	F4	F5	F6	F7	F8	F9	F10	F11
Dope	D15	D15	D15	D15	D15	D15	D15	D15	D18	D18	D20
Internal coagulant flow rate (mL/min)	1.1	1.1	1.3	1.3	1.4	1.8	1.8	1.5	1.4	1.4	1.5
Take-up velocity (m/min)	4.5	3.9	4.7	4.7	4.9	4.5	4.5	4.5	4.1	3.9	4
Post-treatment by ethanol	No	No	No	Yes	No	No	Yes	No	Yes	Yes	Yes
Outer diameter (mm)	0.898	0.841	0.802	0.798	0.898	0.835	0.819	0.875	0.879	0.876	0.872
Inner diameter (mm)	0.522	0.486	0.477	0.476	0.482	0.526	0.519	0.524	0.520	0.523	0.534
Membrane thickness (μm)	188	178	163	161	208	155	150	176	180	177	172
Mean pore radius (μm)	0.054	0.054	0.067	0.032	0.075	0.068	0.031	0.066	0.072	0.064	0.067
Effective porosity (m^{-1})	456	558	541	1238	298	542	1516	413	121	160	71
Permeability[a](10^{-7} mol/m^2.Pa.s)	37.4	45.1	56.6	56.6	35.7	57.6	66.4	42.9	13.8	16.0	7.45
Critical entry pressure (bar)	8	6.5	6	8	8	6	6	8	13	13	>13.3
Collapsing pressure[b] (bar)	11.5	11	10.5	11	11.5	10	10	11.5	>14.3	>14.3	>14.3
Max. pore radius[c] (μm)	0.037	0.045	0.049	0.037	0.037	0.049	0.049	0.037	0.023	0.023	N.A.

[a] Nitrogen gas permeability obtained at a pressure difference of 1 bar and (25 ± 1)°C.
[b] Max. pressure provided by the testing system is 14.3 bar.
[c] Max. pore radius was estimated based on the Laplace equation using CEP_w values.

diameter of 0.8 mm and a tube inner diameter of 0.22 mm. Water was used as both internal and external coagulants at ambient conditions (25°C ± 1°C, RH = 60–65%). Other controlled spinning conditions include internal coagulant rate, dope extrusion rate and take-up velocity. During spinning, the take-up velocity was kept as the same as the free-falling velocity of the nascent fiber to prevent stretching of the fibers. The spun hollow fibers were soaked in fresh water for about 7 days to ensure complete removal of the solvent and additives. Some of the fibers were post-treated via nonsolvent exchange method using ethanol for 1 h to replace water inside the wet membranes before the fibers were finally dried at ambient conditions (25°C ± 1°C and RH ≈ 65%). The details of the spinning conditions for the 11 hollow fibers (F1 to F11) are summarized in Table II.

Characterization of hollow fiber membranes

The prepared PVDF hollow fiber membranes were characterized in terms of morphology, permeability, and hydrophobicity. Scanning electronic microscopy (SEM) (JSM 5600LV) and field emission scanning electronic microscopy (FESEM) (JEOL JSM-6700F) were used to examine the morphology of the spun PVDF hollow fiber membranes by the standard methods. The SEM and FESEM micrographs of cross-section, internal and external surfaces of the hollow fiber membranes were taken at various magnifications. Gas permeation tests were carried out to determine pore structural parameters of the hollow fiber membranes. The apparatus and the detailed procedures of measurements were described elsewhere.[15] In this work, nitrogen with a purity of 99.99% (supplied by SOXAL Singapore) was used as the test gas. Operating pressures were increased stepwise from 200 to 1400 mbar gauge pressure at room temperature (25°C ± 1°C). The membrane's pore structural parameters in terms of effective surface porosity and mean pore radius were obtained by regression of the nitrogen permeance data as a function of average pressure. Hydrophobicity of the membranes was evaluated in terms of the critical entry pressure (CEP), which is defined as the trans-membrane pressure difference at which liquid penetrates pores of the membrane. The detailed procedure of measurement of the critical entry pressure of water (CEP_w) can be found elsewhere.[16] The collapsing pressure of the hollow fiber membranes was also determined. After the CEP_w measurement, the operating pressure was further increased at a 0.5-bar interval and also maintained for 30 min at each pressure level. The pressure at which a hollow fiber was deformed or collapsed was considered to be the collapsing pressure of the membrane. The contact angle of water on the PVDF hollow fiber membrane was measured according to Wilhelmy method[17] using a single fiber tensiometer (K14, Krüss, USA).

Vacuum membrane distillaiton

Five hollow fiber membrane modules (M1–M5) were fabricated from fibers prepared under different conditions. A hollow fiber membrane module was prepared by randomly packing the chosen hollow fibers inside a stainless tube connected to a swagelok at each end, which was sealed with an epoxy resin (UKR-135 resin with UKH-136 hardener, supplied by UK Epoxy Resins).

The schematic flow diagram of the experimental setup and detailed procedure for the vacuum membrane distillaiton (VMD) process are described elsewhere.[16] For each of the membrane modules, VMD

experiments were conducted using both pure water and a binary solution of TCA/H_2O as feed solution. The TCA aqueous solution was prepared by stirring a desirable amount of TCA in a covered 2-L volumetric flask using a magnetic stirrer for at least 3 h until complete dissolution of TCA. Thereafter, the TCA solution was quickly transferred into stainless steel pressure feed tank and sealed. At the beginning and the end of each run, the concentrations of the solution inside the feed tank were measured by taking samples through a sample valve. The feed solution was preheated through a stainless-steel coil and then fed into the lumen side of the module to provide better liquid distribution and improve liquid-membrane contact. At the end of each VMD run, the condensed water and VOC were defrosted and weighted at the room temperature. The TCA concentrations in the feed, retentate and permeate solutions were monitored using a Total Organic Carbon analyzer (TOC-5000A). During the transfer, dilution and measurement of the TCA solution, all the containers used were properly capped, sealed and chilled if necessary to prevent loss through TCA vaporization into atmosphere. For each membrane module, pure water VMD experiment was first conducted according to the same experimental procedures described for TCA-water system, except that in these experiments, only the water condensed in both cold traps needed to be measured. For a doubtful experimental data, the same experiment was repeated until the relative difference was lower than 15%. The relatively large extent of uncertainty of measurement is due both to the low TCA level used in the experiments and its high volatility.

Permeation fluxes (g/m^2 h) of water and of TCA were calculated from the mass and TCA concentration of the condensate collected in the ice-cold trap and liquid-nitrogen cold trap. The TCA flux (J_v) and water flux (J_w) are expressed as:

$$J_v = \frac{W_1 x_1 + W_2 x_2}{A_m t} \tag{1a}$$

and

$$J_w = \frac{W_1(1 - x_1) + W_2(1 - x_2)}{A_m t} \tag{1b}$$

where W_1 and W_2 are the weights of the ice-cold trap condensate and the liquid-nitrogen cold trap condensate respectively, g; x_1, and x_2 are the weight fractions of TCA in the ice-cold trap condensate and in the liquid-nitrogen cold trap condensate, respectively; A_m the membrane area, m^2: $A_m = 2n\pi L(R_o - R_{\text{in}})/\ln(R_o/R_{\text{in}})$ in which R_o and R_{in} are the outer and the inner radius of the hollow fiber, respectively, m; n the number of hollow fibers; and t the operating time, h.

The TCA removal efficiency R_v is defined as:

$$R_v = (1 - c_{A,\text{out}}/c_{A,\text{in}}) \times 100\% \tag{2}$$

where $c_{A,\text{in}}$ and $c_{A,\text{out}}$ are the concentrations of TCA in the feed and retentate solutions in mg/L, respectively.

The separation factor is calculated using the expression:

$$a = \frac{[x_v/x_w]^p}{[x_v/x_w]^f} \tag{3}$$

where x_v and x_w are the weight fraction of TCA and water, respectively. The superscripts p and f refer to permeate and feed, respectively.

RESULTS AND DISCUSSION

Polymer dope composition and viscosity

PVDF dope solutions with three different compositions (D15, D18, and D20) were prepared using DMAc as a solvent and a mixture of water and lithium chloride as nonsolvent additives. The content of PVDF polymer in the dope solutions increased from 15 to 20 wt % as shown in Table I. The measured viscosity data was also listed in Table I. The viscosity of polymer dope increased twofold when the concentration of PVDF was increased from 15 to 18 wt % and further increased by 22% when PVDF concentration was increased from 18 to 20 wt %.

Spinning conditions and PVDF hollow fiber membranes

Eleven batches of PVDF hollow fibers (F1–F11) were prepared from the three different polymer dopes (Table II) by wet-phase inversion method under different spinning conditions using tap water as both internal and external coagulants. The spinning conditions and the properties of the resulting membranes are summarized in Table II. The outer and inner diameters of the dried membranes were measured from SEM micrographs of the cross-section of the fibers. For each batch of the fiber, at least eight readings were taken along the inner and outer circles to obtain the average values.

All the spun PVDF porous hollow fibers exhibited good integrity with good mechanical strength. They generally displayed concentric structure with uniform wall thickness and their measured collapsing pressures are relatively high. In general, the fiber wall thickness increased with increasing PVDF concentration in the dopes. However, it was found that the thickness of the hollow fibers was also affected by the fiber take-up velocity and internal coagulant flow

rate. A comparison of the measured data between pairs of fibers F1 and F2, F3 and F5, and F9 and F10 in Table II reveals that the thickness increased with the increment of take-up velocity. In the spinning of these fibers, the take-up velocity of the hollow fibers was maintained nearly the same as the free falling velocity of the fiber in the coagulation bath to prevent the extension of the fibers by mechanical drawing. This means the take-up velocity was adjusted according to the dope extrusion rate during the hollow-fiber spinning process. Therefore, the take-up velocity was a manifestation of the extrusion rate. A higher take-up velocity reflects a higher dope extrusion rate which means more PVDF polymer was extruded into the coagulation bath within the same time period and resulted in a thicker fiber wall after coagulation, when other spinning conditions remained unchanged. On the other hand, an increase in internal coagulant flow rate resulted in a decrease of membrane thickness. For instance, when the internal coagulant flow rate increased from 1.1 to 1.5 and further to 1.8 mL/min, the corresponding thickness of hollow-fibers F1, F8, and F6 reduced from 188 to 176 and further to 155 μm. It is interesting to note that the increase of the inner diameter of the fiber caused by increasing internal coagulant flow rate was not significant, while the reduction of the outer diameter of the fiber was the major reason for the reduction of the fiber wall thickness. It appears that the higher internal coagulant rate, which means higher inner coagulant (H_2O) driving force for mass transfer through the inner porous surface and resulted in higher H_2O content within the inner layer of the wall. This could have retarded the movement of coagulation front moving towards the center of the fiber wall due to the influx of coagulant (also H_2O) from external coagulation bath.

Gas permeation tests

The mean pore radius (r_p) and effective surface porosity (ε/L_p) of the spun hollow fibers were determined by gas permeation test. The effective surface porosity is defined as surface porosity per effective pore length of the thin skin layer of a hollow fiber. For an asymmetric membrane, the resistance of the porous supporting structure can be neglected. The gas permeation is determined mainly by the resistance of the microporous selective layer at the outer edge of the hollow fiber. The measured mean pore radius, effective surface porosity and nitrogen gas permeability at a pressure difference of 1 bar and (25 ± 1)°C of the 11 hollow fibers are also listed in Table II.

Over the concentration range of PVDF in the dope, no apparent effect on the mean pore size of the prepared hollow fibers is shown; however, a significant reduction of the effective porosity and nitrogen gas permeability of the membranes is depicted. When the PVDF dope concentration increased from 15 to 20 wt %, the effective surface porosity reduced from as high as 1516 to 71 m^{-1} and the nitrogen gas permeability reduced from 66.4×10^{-7} to 7.45×10^{-7} mol/m^2 Pa s. The reduction of porosity of the membrane could also be attributed to the decrease of the amount of the additive in the dopes. It has been reported in other studies that an increasing amount of small-molecule additive in the dope solution can result in an increase of porosity of the spun fiber.[13,18,19] In this study, the amount of additives indicated by gram additives per 100 g of solution was slightly reduced with an increase of PVDF concentration in the dope solutions to make the change of membrane morphology more significant.

Post-treatment of the spun fiber using ethanol caused a significant increment of the surface porosity and enhanced the rate of permeation of nitrogen gas. The most possible reason was that a post-treatment of the membranes with a low-surface tension nonsolvent, such as ethanol, may help to prevent collapse and closure of pores when the nonsolvent evaporated into the atmosphere during drying of the fibers.

Gas permeability is related to membrane thickness (δ), which as discussed above, is determined by the dope composition and spinning conditions, e.g. extrusion rate and internal coagulant flow rate. In general, the nitrogen gas permeability is observed to be inversely proportional to the membrane thickness in this study as illustrated in Figure 1, for hollow fibers spun from 15 wt % PVDF dope. However, the inversed relationship between nitrogen gas permeability and

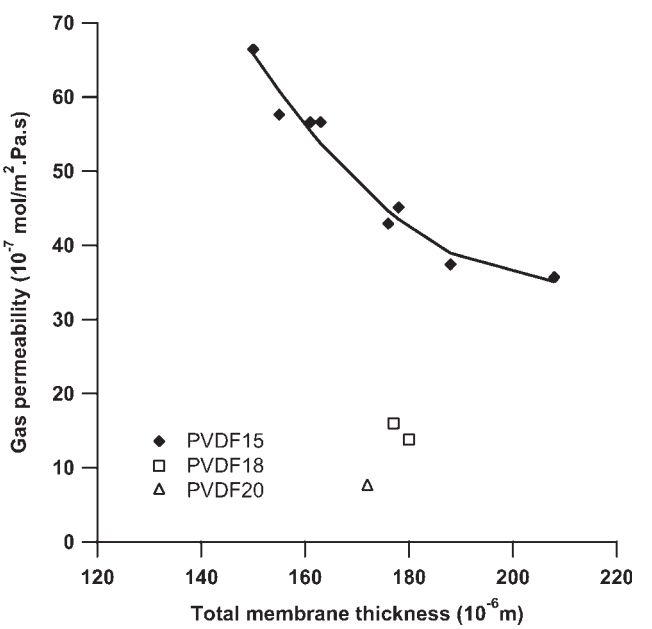

Figure 1 Nitrogen gas permeability versus total thickness of PVDF hollow fiber membranes. (Gas permeability was obtained at pressure difference of 1 bar and temperature of 25°C ± 1°C).

total membrane thickness broke away when the thickness was further increased from 190 to 210 μm. Theoretically, for the dense and homogenous membrane, the gas permeability should be inversely proportional to the membrane thickness. While for the microporous asymmetric membrane, the gas permeability is assumed to be inversely proportional to the effective pore length, which can be considered as a product of the tortuosity and thickness of thin selective layer. However, due to the asymmetric structure and complicated morphology of the microporous membrane, it is difficult to relate the gas permeability directly to its total geometric thickness. The results in this study show that increment of total membrane thickness results in a proportional increase of the effective thickness of the selective layer which leads to the increase in gas transport resistance. However, a further increase of the membrane thickness did not reduce the permeability of the membrane in the same manner. The further thickness increment could be contributed mainly in the increment of the porous supporting layer which exerts negligible transport resistance. For PVDF membranes spun from 18 (D18) and 20 wt % (D20) dope solutions and with the same thickness as that from 15 wt % (D15) dope, the permeability was only about one third and one sixth of the latter, respectively. The results illustrate that the morphology of the membranes spun from the three different dope concentrations are quite different. Further discussion of the difference in morphology is presented under morphology examination by SEM and FESEM.

CEP, collapsing pressure and contact angle measurement

The hydrophobicity of the PVDF hollow fiber membranes was determined by measuring the CEP and contact angle of water, while the mechanical strength of the membranes was characterized by measuring their collapsing pressures. The CEP and collapsing pressures of the prepared membranes are listed in Table II. The CEP_w on the PVDF hollow fibre membranes increased with the PVDF dope concentration. The hollow fibers spun from 15 wt % PVDF dope have CEP_w ranging from 6.0 to 8.0 bar while fibers spun from 18 wt % PVDF dope exhibited a CEP_w of 13.0 bar. The CEP_w of fibers spun from 20 wt % PVDF dope exceeded the maximum pressure difference provided by the testing system of 13.3 bar and was not detected. The increase in CEP_w with an increase in polymer concentration in dope may be due to the decreased pore size of the resulting membranes. This will be further verified by the determination of maximum pore sizes of the membranes. The CEP_w values of all membranes tested are much higher than the operating pressures employed in VMD experiments. Therefore, the membranes could not in principle be wetted due to the pressure difference in the VMD process. All the hollow-fiber membranes prepared exhibited good mechanical strength with collapsing pressure higher than 10 bar. The collapsing pressure of the membranes was observed to increase with dope solution concentration. For hollow fibers spun from 18 and 20 wt % dope, the collapsing pressures were higher than 14.3 bar, which is the upper limit of our testing system.

In this study, wettability of PVDF membrane by liquid water was also examined by measuring the advancing contact angle of water on the polymer via the Wilhelmy method. The average value of advancing contact angles of water on PVDF fiber (F1) calculated from 10 readings is $(78.4 \pm 1.7)^\circ$. The measured values are consistent with the values of 75–82.3° reported by other reseachers.[20–23] The difference of water contact angle among the membranes was within the standard deviation of the measurement.

The maximum pore radius of the membranes, $r_{p,\max}$, can be estimated from the measured water contact angle and CEP_w according to the Laplace equation:

$$r_{p,\max} = \frac{2\gamma B \cos\theta}{CEP_w} \tag{4}$$

where γ is the liquid surface tension, N/m, B is a geometric factor determined by the pore structure, and θ is the liquid-solid contact angle. B is equal to 1, when the pores are assumed to be cylindrical. The results are listed in Table II. It was found that the maximum pore radius estimated from the Laplace equation is in the same order of magnitude as the mean pore radius determined by gas permeation tests. The mean pore radius measured by gas permeation tests, which ranges from 0.031 to 0.075 μm for all prepared membranes, does not appear to show any significant correlation to the PVDF dope concentration. However, by the estimation from CEP_w value, the values of maximum pore radius of membranes spun from 15 wt % dopes range from 0.037 to 0.049 μm compared to 0.023 μm measured from membrane prepared from 18 wt % dope solution.

Morphology examination by SEM and FESEM

The morphology of the prepared PVDF hollow-fiber membranes was examined by SEM and FESEM with different magnifications. In general, the spun hollow-fiber membranes had a highly asymmetric structure, good geometrical shape, and good integrity. The internal and external surfaces of the hollow fibres were spun to be nearly concentric circles to ensure a uniform fiber wall thickness. The typical morphology of the resulting membranes is presented in Figure 2,

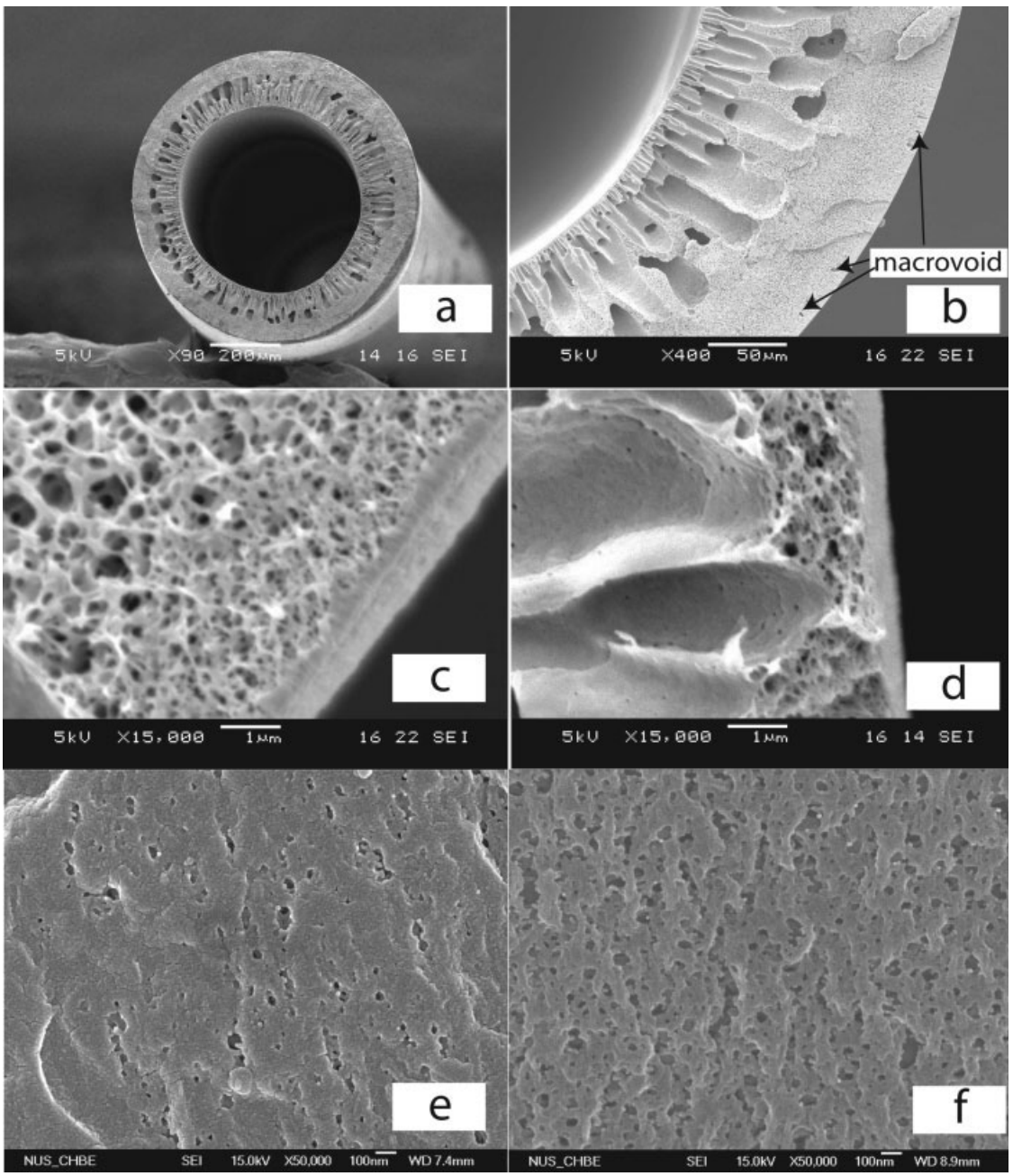

Figure 2 SEM and FESEM photographs of fiber F6: (a) total cross section; (b) partial cross section; (c) outer edge of cross section; (d) inner edge of cross section; (e) external surface; (f) internal surface (magnification of internal and external surface is 50,000).

which illustrates the SEM and FESEM micrographs of the cross section, internal and external surface of the fiber (F6). As shown in the cross-section photographs, the hollow-fiber membranes have five layers of different structures from the external to internal surface including (i) an external thin dense skin layer with a thickness of ~1 μm, (ii) a layer of small macrovoids with length of about 10 μm laying closely beneath the top skin layer and discretely distributing within the sponge-like structures, (iii) a layer of sponge-like structure with inter-connecting pores, (iv) a thick finger-void structures with a thickness of about half of the total fiber thickness, and (v) a sponge-like structure with a thickness less than 4 μm forming the internal surface. It is also shown that the external surface of the hollow-fiber has micropores discretely distributed while the internal surface is highly porous with network-pore structure.

The effect of post-treatment on the membrane morphology can be found by comparing the SEM and FESEM photographs of hollow fibers F6 (without post-treatment) and F7 (with post-treatment) as

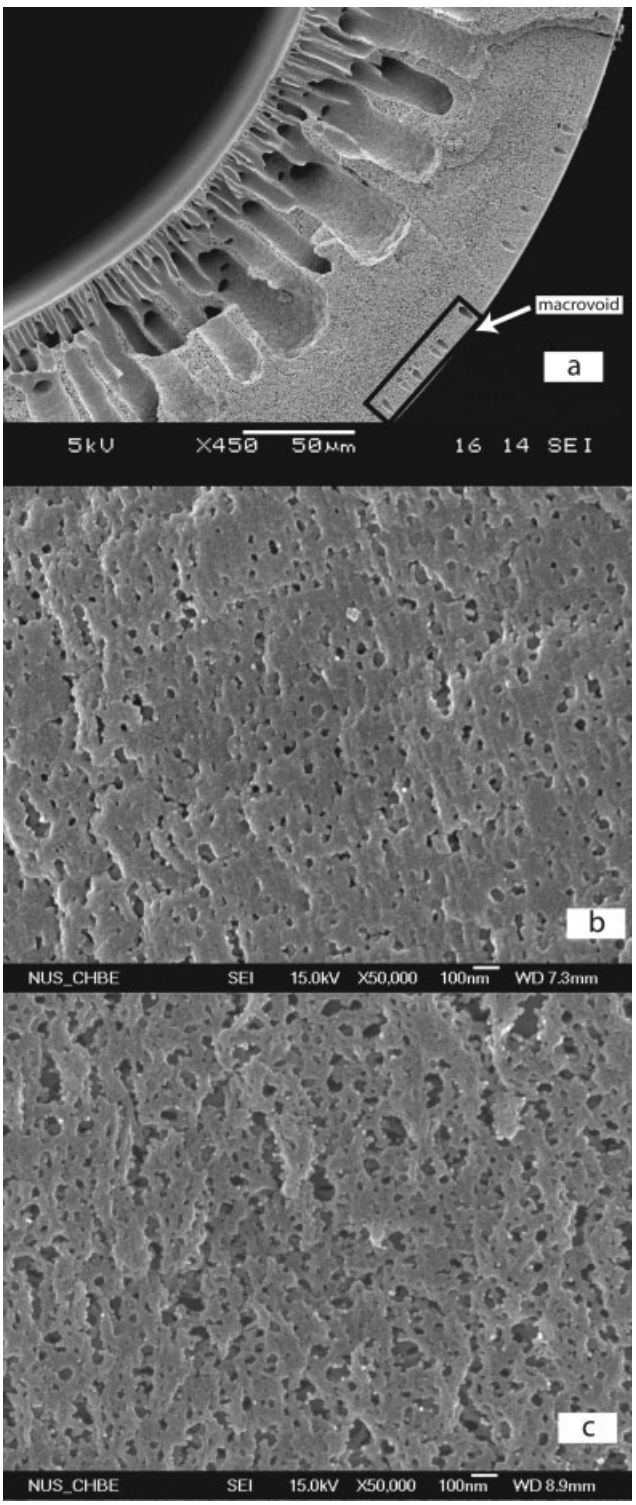

Figure 3 SEM and FESEM photographs of fiber F7: (a) partial cross section; (b) external surface; (c) internal surface (magnification of internal and external surface is 50,000).

shown in Figures 2 and 3. One apparent change was that the external surface of the membrane became more porous after the post-treatment by the ethanol. It was also found that the micropores of F7 were distributed evenly on the external skin while those of F6 were concentrated in some areas. These results further confirm that the ethanol post-treatment reduced the collapse and closure of pores and the membrane shrinkage during the air-drying process.

The effect of dope concentration on the membrane morphology was also examined by the SEM and FESEM micrographs. As depicted in Figure 4, hollow fibers spun from 18 and 20 wt % dope generally have similar morphology as that from 15 wt % dope. However, the membrane structure changes moderately with increment of dope concentration. The layer of small macrovoids beneath the top skin layer found in fiber prepared with 15 wt % dope disappear in fibers F10 (18 wt % dope) and F11 (20 wt % dope). This could be due to the reduced tolerance of water within dope solutions with increasing polymer concentration, which results in a fast solidification of the outer skin layer and causes the layer of small microvoids to have no time to develop. It was also noted that the demixing front shifted slightly to the inner surface and the thickness of finger-void layer reduced. A significant change of the membrane morphology with dope concentration was the reduced pore size and surface porosity on the external surface of the membranes (see also data for F10 and F11 in Table III).

From the FESEM micrographs, the dimension of the pores could be measured using a computer software named Smile View and recorded. The mean pore size was determined based on the number of pores and their diameters measured over a selected membrane area. The surface porosity is defined as the ratio of total pore area to total selected membrane area. The data presented in Table III includes both the mean pore radius and porosity on the external and internal surface of six selected membranes. The mean pore radii on both the external and internal surfaces of the hollow fibers are in the range of 10^{-8} m (0.01 μm), which are consistent with the results obtained from the gas permeation test and the maximum pore size method based on the CEP_w. However, the mean pore radii determined by gas permeation test are generally larger than those measured from the FESEM micrographs. The mean pore size and surface porosity of internal surface measured from the FESEM micrographs are about 1.1–1.5 times and 2.2–5.0 times as large as those of external surface, respectively. Therefore, the selective layer of the hollow fiber membranes is the outer surface. However, the mass transfer resistance through the internal surface may not be totally negligible since its pore size and porosity is comparable to that on the external surface. Therefore, in this study, the logarithmic mean radius of the hollow fiber is used to estimate the effective membrane area, which is being used to calculate the permeation fluxes of TCA and water as shown in eqs. (1a) and

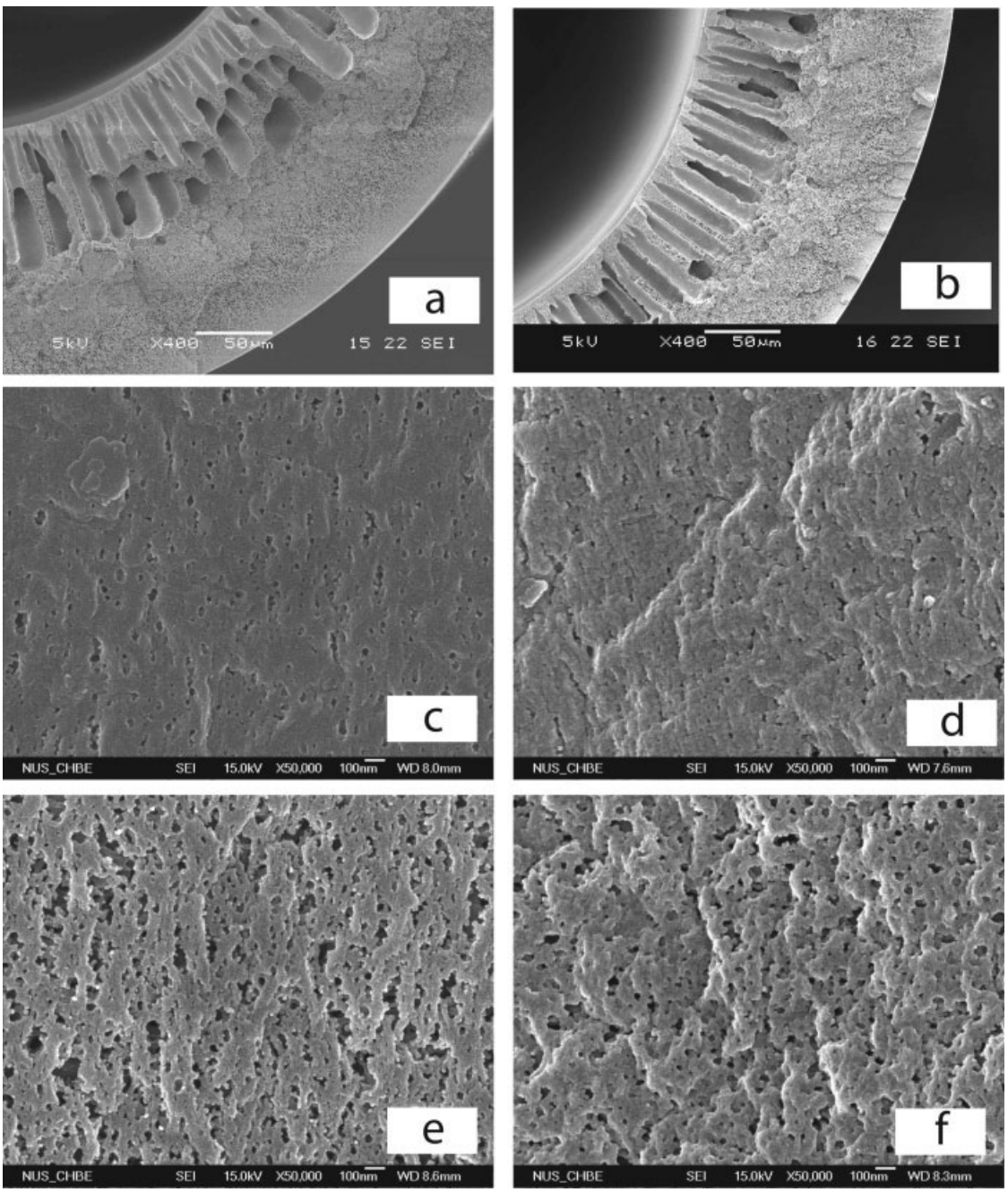

Figure 4 SEM and FESEM photographs of fibers F10 and F11: (a) partial cross section of F10; (b) partial cross section of F11; (c) external surface of F10; (d) external surface of F11; (e) internal surface of F10; (f) internal surface of F11 (magnification of internal and external surface is 50,000).

(1b). Based on the SEM methods, the mean pore size and surface porosity generally decrease with the PVDF concentration of the dope. This result is consistent with those obtained from gas permeation test and maximum pore size estimation.

The discrepancy of the mean pore sizes determined by the three different methods may arise from the different theoretical backgrounds and experimental uncertainty of each method. Shin et al.,[24] had indicated that the magnitude of mean pore size determined by gas permeation does not have any significant physical meaning for the membranes prepared by phase inversion method. As discussed in the above Section on gas permeation test, there appears to have no correlation between the mean pore size of the prepared hollow fibres and the properties of PVDF dope and also the spinning conditions. Moreover, there was no observed effect of mean pore size on gas permeation properties which depends mainly on effective porosity.

TABLE III
Mean Pore Size and Surface Porosity Determined by FESEM Micrographs

Hollow fibre	F1	F6	F7	F8	F10	F11
Mean pore radius on external surface (μm)	0.015	0.015	0.014	0.013	0.011	0.008
Surface porosity on external surface (%)	4.84	7.98	13.4	10.1	9.01	3.03
Mean pore radius on internal surface (μm)	0.017	0.017	0.018	0.016	0.015	0.011
Surface porosity on internal surface (%)	24.1	30.4	33.3	22.2	30.4	8.42

VMD experiments

Five membrane modules (M1–M5) were prepared from selected PVDF hollow-fibers (F1, F6, F7, F10, and F11, respectively). The properties of membrane modules are listed in Table IV. Among the membrane modules, modules M2–M5 have housing tubes with the same dimensions, whereas module M1 has a housing tube with the same ratio of inner diameter to length as those of M2–M5, but has a total membrane area approximately three times of the others. All the membrane modules have the same packing density.

VMD experiments using pure water

To study the effects of membrane parameters on the permeation flux, pure water VMD experiments were first conducted using modules M2–M5. The downstream pressure was varied from 80 to 40 mmHg (106.7–53.3 mbar) with all the other operational conditions remaining unchanged at a feed temperature of 50°C and a feed flow rate of 10^{-3} m^3/h.

For gas permeation through microporous membrane in a VMD process, mass transfer by permeation through the membrane maybe due to both Knudsen diffusion and viscous flow. However, under the experimental conditions employed in this study, the mean-free-paths of water molecules calculated range from 1.2 to 1.6 μm, which is much larger than the mean pore sizes of the membranes which are in the order of about 0.01 μm. This suggests that the Knudsen diffusion is the dominant mass transfer mechanism through the membrane pores in VMD. A more detailed description of the mechanism of permeation is given elsewhere.[3]

For Knudsen diffusion, the molar flux across the membrane is expressed as

$$N_i = \frac{2r_p\varepsilon}{3\tau RT}\left(\frac{8RT}{\pi M_i}\right)^{1/2}\frac{\Delta P_i}{\delta} \tag{5}$$

where N_i is the molar flux of gas, mol/m^2.s; r_p is the mean pore radius of the pore, m; ε is the membrane surface porosity; τ is the pore tortuosity; δ is the membrane thickness; M_i is the molecular weight of gas, kg/mol; R is the gas constant; T is the absolute temperature, K; ΔP_i is the partial pressure difference between the upstream and downstream of the membrane. For a given permeating species through a membrane at a given temperature, permeation flux is directly proportional to the partial vapor pressure difference ΔP_i across the membrane. As there is slight difference in bulk temperature of the inlet and the outlet stream (i.e. less than 1.0°C) measured in pure water VMD experiments, the thermal boundary layer at the upstream of the membrane is assumed to be negligible. A logarithmic mean pressure difference ΔP_{lm} is used and is given by the following expression:

$$\Delta P_{\mathrm{lm}} = \frac{[P^s_w(T_{b,\mathrm{in}}) - P_p] - [P^s_w(T_{b,\mathrm{out}}) - P_P]}{\ln\{[P^s_w(T_{b,\mathrm{in}}) - P_p]/[P^s_w(T_{b,\mathrm{out}}) - P_P]\}} \tag{6}$$

where P^s_w is water vapor pressure (Pa), which is related to the temperature by using Antoine equation: $P^s_w(T) = \exp\left(23.1964 - \frac{3816.44}{-46.13+T}\right)$, T is in K; $T_{b,\mathrm{in}}$ and $T_{b,\mathrm{out}}$ are the bulk temperature at the inlet and outlet of the membrane module; P_p is the vapor pressure at the permeate side.

TABLE IV
Properties of the PVDF Hollow-Fibre Membrane Modules

Membrane module	M1	M2	M3	M4	M5
Hollow fiber	F1	F6	F7	F10	F11
Inner diameter of the housing tube (m)	1.6×10^{-2}	1.1×10^{-2}	1.1×10^{-2}	1.1×10^{-2}	1.1×10^{-2}
Inner diameter of the hollow fibers (mm)	0.52	0.53	0.52	0.52	0.53
Outer diameter of the hollow fibers (mm)	0.90	0.84	0.82	0.88	0.87
Thickness of the membrane, δ (μm)	188	155	150	177	172
Mean pore radius of the membrane, r_p (m)	5.4×10^{-8}	6.8×10^{-8}	3.1×10^{-8}	6.4×10^{-8}	6.7×10^{-8}
Effective porosity of the membrane, ε/L_p (m^{-1})	456	542	1516	160	71
Effective length of the fibers, L (m)	0.51	0.33	0.33	0.33	0.33
Number of the hollow fibers, n	143	71	73	68	68
Packing density (m^2/m^3)	2000	2000	2000	2000	2000
Total membrane area, A_m (m^2)	0.159	0.0492	0.0498	0.0482	0.0486

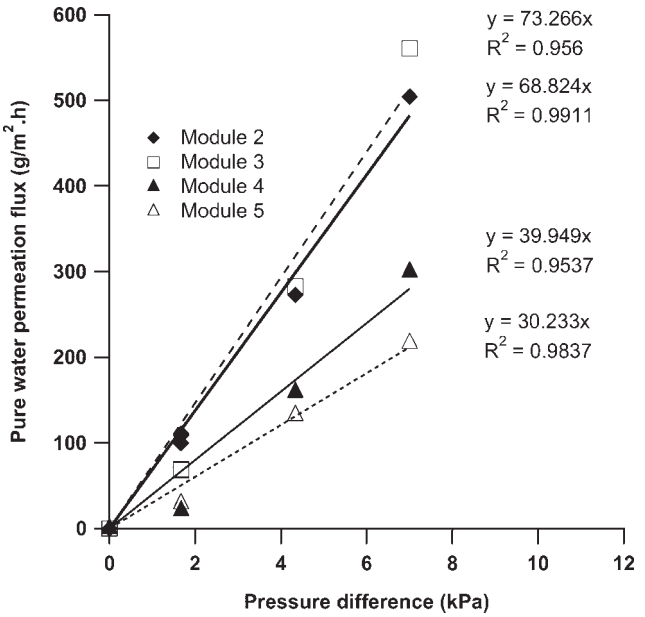

Figure 5 Pure water permeation flux versus pressure difference between feed bulk and permeate side in VMD. Downstream pressure, 40–80 mmHg; feed temperature, 50°C; feed flow rate, 10^{-3} m^3/h.

When the measured water permeation fluxes are plotted against ΔP_{lm} as depicted in Figure 5, a linear relationship was obtained for all the different modules employed. As stated earlier, the Knudsen diffusion is assumed to be the dominant mass transfer mechanism in pure water VMD process due to the mean-free-paths of water molecules being much larger than the mean pore sizes of the membranes. This observed linear behavior of permeation flux with ΔP_{lm} confirms further that Knudsen diffusion is the mechanism responsible for mass transport through the membrane pores in pure water VMD process, whereas the contribution due to viscous flow is negligible.[3,25]

The slope of the straight line can be considered as a global membrane distillation (MD) coefficient, which is related to the VMD operational temperature and membrane parameters. The calculated values of global MD coefficient of the tested membranes range from 30.2 to 73.3 $g/m^2.h.kPa$ which follows the order of decreasing pore sizes and effective surface porosity of the hollow fibers according to the sequence: F7 > F6 > F10 > F11. These results are also consistent with those of gas permeability data determined from gas permeation tests (Table III).

TCA/water VMD experiments

VMD experiments involving TCA-Water system were conducted using all the five membrane modules at a TCA feed concentration of 430 ppm with all the other operating conditions remaining the same as those in pure water VMD experiments. In all the experiments, phase separation phenomenon was observed in the liquid nitrogen cold trap after the condensate was defrosted. Droplets of TCA were immersed at the bottom of the aqueous solution in liquid nitrogen cold trap and can be easily removed and recovered from the aqueous solution. The effects of various operating conditions, i.e. feed solution temperature, downstream pressure, feed flow rate and feed concentration, on the performance of VMD in VOC removal have been studied in detail and the results have been reported elsewhere.[16] In this study, the objective is to investigate the effect of membrane parameters, i.e. the mean pore size and effective porosity, and the membrane module parameters, i.e. the total membrane area and module length, on the performance of VMD process. Therefore, only the downstream pressure was changed to observe the variation of water and TCA permeation flux, TCA removal efficiency and separation factor of the different membrane modules. The results are illustrated in Figure 6.

Water permeation flux was affected by both the membrane parameters and the membrane module parameters. For the four modules M2–M5, the water permeation flux generally increased with increasing membrane effective surface porosity and gas permeability in accordance of the sequence of modules M5(F11) < M4(F10) < M3(F7) ≈ M2(F6). At the operating temperature of 50°C, the flux generally increased dramatically with reducing operating pressure of the VMD process. The operation of VMD process at too low a pressure is not desirable as the high water flux reduced significantly the VOC concentration in the permeate stream and increased energy consumption. It is interesting also to compare the water permeation flux of the smaller modules (M2–M5) with the bigger module M1 with the same packing density and under the same operating conditions. The former generally exhibited a much higher water permeation flux than the latter. At the same liquid feed rate of 10^{-3} m^3/h through the lumen side of the hollow fibers, the bulk liquid velocity in the smaller modules with less hollow fibers is higher than the bigger modules with more fibers. The higher liquid velocity could cause a reduction in both the mass and heat transfer resistance in the liquid boundary layer and provide more efficient heat transfer for the evaporation of water and TCA at the liquid-membrane interface and the mass transfer of the vapors through the membrane. For example, the calculated Reynolds numbers for modules M1 and M2 are 8.6 and 17.0, respectively.

The difference of TCA permeation fluxes caused by the membrane parameters is less significant for the smaller modules M2 to M5 as shown in Figure 6(b) except M3. The latter which exhibited the highest per-

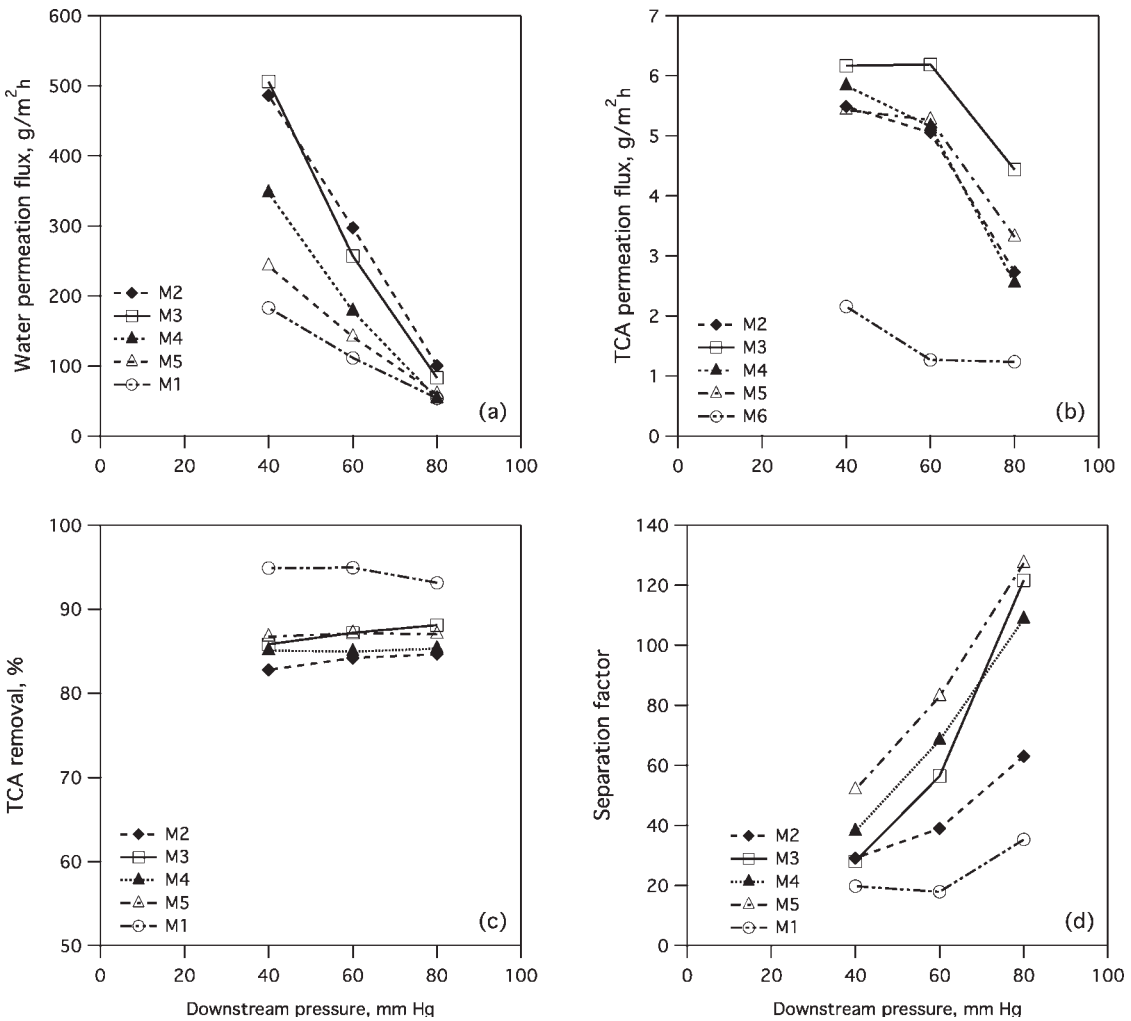

Figure 6 Effect of downstream pressure on: (a) water permeation flux; (b) TCA permeation; (c) TCA removal; (d) separation factor, in VMD for membrane modules M1–M5. The TCA feed concentration, 430 ppm; feed temperature, 50°C; feed flow rate, 10^{-3} m^3/h.

meation flux, was fabricated using hollow fiber F7 which displayed the largest effective porosity of 1516 m^{-1} and the smaller mean pore radius of 3.1 $\times$ 10^{-8} m among all the modules tested (Table IV). The permeation data for the larger module, M1 are substantially lower than all the smaller modules operating under the same conditions. The phenomenon is the same as the water permeation flux, as discussed above is due to the lower bulk liquid velocity which significant reduced the mass and heat transfer efficiency. It is also possible that in the presence of more hollow fibers in the bigger module the membrane area was not utilized as efficiently as in smaller modules with fewer fibers due to less uniform liquid distribution per unit membrane area.

In terms of TCA removal efficiency by the different membrane modules as presented in Figure 6(c), the results reveal generally, that the smaller modules have the similar TCA removal efficiency varying from 83 to 88% under different downstream pressures. As anticipated, the larger module M1 with three times the membrane area as compared to the smaller modules yielded higher TCA removal efficiencies ranging between 93 to 95%. The effect of operating pressure is generally marginal in all cases.

The separation factor of TCA, as defined by Eq. (3), for the different membrane modules under different downstream pressures are presented in Figure 6(d). As shown, the data of TCA separation factor for the four smaller modules M2–M5 generally follow the reverse trend of water permeation flux [Fig. 6(a)] with respect of both membrane parameters as well as operating downstream pressure with the exception of M3. The separation factor increased significantly with decreasing effective porosity but with increasing operating downstream pressure in the permeate side. It appears that the membrane prepared from the higher

polymer-concentration dope exhibits a higher TCA separation factor with the exception of module M3. As mentioned above, the module M3 fabricated from hollow fiber F7 spun from a membrane dope of 15 wt % PVDF has a very high effective porosity with the smallest pore size among all the membranes. Its TCA separation factor was affected dramatically by the downstream vacuum level. When the downstream pressure was relatively high at 80 mmHg which is just slightly lower than the water saturation pressure at 50°C (92.5 mmHg), M3(F7) exhibited not only the highest TCA permeation flux but also nearly the highest separation factor among all the modules tested. However, with the reduction of the downstream pressure, the greatly enhanced water permeation flux reduced significantly the TCA concentration in the permeate stream thus its separation factor. Similar trend of operating pressure dependency also applies to the other three smaller modules. As expected, the larger membrane module M1 displayed the lowest separator factor due to its relatively inefficient mass and heat transfer at the liquid-membrane interface caused by the low Reynolds number.

In the VMD process to remove TCA from its aqueous solutions using different microporous PVDF membranes, the pore size and porosity of the membranes seem to affect the selectivity of membrane to TCA. The results imply that the Knudsen diffusion may not be the only mass transfer mechanism in VMD processes for VOC removal. The affinity between the VOC molecules and the PVDF polymer may also contribute to the selectivity of the membranes in the VMD processes. The sorption of TCA molecules in PVDF polymer needs be further studied in future. The mechanism of solution-diffusion through the nonporous portion of the membrane may play a role in vapor transport through the membrane. For example, the higher separation factor of M5 and M4 modules is obviously due to the denser membrane (lower surface porosity) which exhibited higher selectivity due mainly to solution-diffusion mechanism.

In general, although a low operating pressure favors both water vapor and TCA permeation flux. However, the overwhelming water vapor permeation flux at low pressure is undesirable as not only it reduces the concentration of the VOC in the permeate stream, but also it will consume extra energy for vaporization. The highly porous membrane should be operated under a pressure close to the water saturation pressure in VMD process to get both high separation factor and high TCA permeation flux. The membrane module could be used more efficiently to achieve both higher permeation flux and TCA separation factor by optimizing the total membrane separation area or the size of the membrane module, with a compromise of TCA removal percentage.

CONCLUSIONS

Asymmetric microporous PVDF hollow-fiber membranes with good hydrophobicity and integrity have been prepared by phase inversion methods using DMAc as a solvent and a mixture of LiCl and water as a nonsolvent additive. Membranes with different mean pore sizes, effective porosities, and morphologies were prepared by varying the dope concentration and spinning conditions. The results reveal that variation of the polymer dope compositions offers the most significant effect on the morphology and permeation characteristics of the resulting hollow fiber membranes. An increase in polymer dope concentration led to a reduction of effective surface porosity and mean pore size on both the external and internal surfaces as well as nitrogen gas permeability. For the hollow fiber membranes spun from the same dope composition, the gas permeability was closely related to the total membrane thickness, which can be controlled by the internal coagulant flow rate and/or the dope extrusion rate. Post-treatment by nonsolvent exchange using ethanol increased the effective surface porosity and prevented pore collapse and closure due to the membrane shrinkage during air-drying.

The global MD coefficients of different membrane modules were determined based on pure water VMD experiments. A good linear dependence of water flux on the transmembrane vapor pressure difference indicates a Knudsen-dominant mass transfer mechanism through the porous membranes in pure water VMD. Results from TCA/water VMD experiments reveal generally that membranes with lower effective porosity displayed higher VOC separation factor but at a reduced VOC permeation flux. A highly porous hollow fiber membrane with a smaller mean pore size can achieve both high TCA permeation flux and high separation factor. It is desired for the VMD process to be operated at a downstream pressure close to the saturated pressure of water at the operating temperature.

References

1. Bodell, B. R. U.S. Pat. 285,032 (1963).
2. Findley, M. E. Ind Eng Chem Process Des Dev 1967, 6, 226.
3. Lawson, K. W.; Lloyd, D. R. J Membr Sci 1997, 124, 1.
4. Burgoyne, A.; Vahdati, M. M. Sep Sci Technol 2000, 35, 1257.
5. Curcio, E.; Drioli, E. Sep Purif Rev 2005, 34, 35.
6. Khayet, M.; Mengual, J. I.; Matsuura, T. J Membr Sci 2005, 252, 101.
7. Wu, Y.; Kong, Y.; Lin, X.; Liu, W.; Xu, J. J Membr Sci 1992, 72, 189.
8. Kong, Y.; Lin, X.; Wu Y.; Chen, J.; Xu, J. J Appl Polym Sci 1992, 46, 191.
9. Fujii, Y.; Kigoshi, S.; Iwatani, H.; Aoyama, M.; Fusaoka, Y. J Membr Sci 1992, 72, 53.
10. Fujii, Y.; Kigoshi, S.; Iwatani, H.; Aoyama, M.; Fusaoka, Y. J Membr Sci 1992, 72, 73.

11. Ortiz de Zárate, J. M.; Peña, L.; Mengual, J. I. Desalination 1995, 100, 139.
12. Tomaszewska, M. Desalination 1996, 104, 1.
13. Khayet, M.; Matsuura, T. Ind Eng Chem Res 2001, 40, 5710.
14. Deshmukh, S. P.; Li, K. J Membr Sci 1998, 150, 75.
15. Wang, D.; Li, K.; Teo, W. K. J Membr Sci 1995, 105, 89.
16. Wu, B.; Tan, X.; Teo, W. K.; Li, K. Sep Sci Technol 2005, 40, 2679.
17. Kwok, D. Y.; Neumann, A. W. In Surface Characterization Methods: Principles, Techniques and Applications; Milling, A. J., Eds.; Marcel Dekker: New York, 1999; p 41.
18. Wang, D. L.; Li, K.; Teo, W. K. J Membr Sci 2000, 178, 13.
19. Kong, J.; Li, K. J Appl Polym Sci 2001, 81, 1643.
20. Owens, D. K.; Wendt, R. C. J Appl Polym Sci 1969, 13, 1741.
21. Nunes, S. P.; Peinemann, K. V. J Membr Sci 1992, 73, 25.
22. Huang, R. Y. M.; Pal, R.; Moon, G. Y. J Membr Sci 2000, 167, 275.
23. Khayet, M.; Chowdhury, G; Matsuura, T. AIChE 2002, 48, 2833.
24. Shih, H. C.; Yeh, Y. S.; Yasuda, H. J Membr Sci 1990, 50, 299.
25. Bandini, S.; Saavedra, A.; Sarti, G. C. AIChE 1997, 43, 398.